Evaluating the 'Reciprocity Failure' of 1.7 Micron Cut-off HgCdTe Photodetectors

Robert Newman

Advisor: Wolfgang Lorenzon

A Thesis presented for the degree of
Bachelor of Science

SNAP Group
Department of Physics
University of Michigan
November 2009

Dedicated to

My parents, whom through all my hyperactive antics as a child, complete lack of direction as an adolescent and multiple major changes as a collegiate student, have always been there for me, physically, mentally, and monetarily, regardless of what sort of crazy path I decided to take. I have been blessed with two of the greatest parents in the world. I love you Mom and Dad.

Evaluating the 'Reciprocity Failure' of 1.7 Micron Cut-off HgCdTe Photodetectors

Robert Newman

Submitted for the degree of Bachelor of Science
November 2009

Abstract

Quantifying dark energy is at the forefront of the scientific community. To better understand and quantify dark energy, high-precision measurements of the expansion of the universe are required. The SuperNova Acceleration Probe (SNAP) is a proposed space mission that would be capable of such high-precision measurements. Utilizing distant supernova and near infrared (NIR) detectors, SNAP can determine the expansion history of the universe over the last 10 billion years to an accuracy of 1% [1]. The NIR detectors on SNAP must meet strict performance specifications. One of these performance specifications is detector linearity at the below 1% level. To achieve this high level of detector linearity the University of Michigan SNAP NIR laboratory designed and manufactured a dedicated experimental setup that accurately characterizes 'reciprocity failure.' Reciprocity failure was originally documented by NICMOS 2005-002 [2], as a 5-6%/dex effect on 2.5 micron cut-off HgCdTe devices. The reciprocity failure of the H2RG SNAP-102 1.7 micron cut-off HgCdTe photodetector at 790nm is less than ±0.25%/dex, which is much smaller than that found on the NICMOS arrays.

Declaration

The work in this thesis is based on research carried out by the University of Michigan SNAP group, in the Department of Physics at the University of Michigan, Ann Arbor. No part of this thesis has been submitted elsewhere for any other degree or qualification and is all my own work unless referenced to the contrary in the text.

Acknowledgements

Without the knowledge, advice and patience of my many colleagues none of this would have been possible.

Curtis Weaverdyck

Wolfgang Lorenzon

Greg Tarlé

Michael Schubnel

Tomasz Biesiadzinski

Rebecca Jackson

Table of Contents

Abstract……...**i**
Declaration……..……**ii**
Acknowledgements…… **iii**
Table of Contents……..... **iv**
List of Figures……**v-vi**

Chapter 1
Overview……..... **1**
Dark Energy…… **1**
SNAP……... **1**
Precision Photometry……... **1**
Precision Photometry at the University of Michigan……... **2**
Reciprocity Failures……..... **2**
The Detector and Photodiodes…… **3**

Chapter 2
Experimental Setup……**4**
Original Design……... **4**
Actual Design……...**5-6**
Encountered Difficulties…….. **7-15**

Chapter 3
Photodiode Calibration……..**16**
Procedure…… **16**
Data Analysis……... **17**
Conclusion……... **18**

Chapter 4
Detector Reciprocity…….. **19**
Procedure…… **19**
Data Analysis……... **20**
Conclusion……... **21**
Conclusion 2……**21**
Laser Reciprocity Procedure……..... **22**
Laser Reciprocity Conclusion……..... **24**
Summary…….. **24**

References……... **25**
Appendix A…… **26**
Appendix B…… **27**
Appendix C…… **28-29**

List of Figures

Chapter 1

Table 1.1 Attributes that must be characterized for precise photometry.

Figure 1.1 Left panel: NICMOS arrays (2.5 μm cut-off HgCdTe) on HST exhibit a 5-6%/dex flux dependent non-linearity. Right panel: The wavelength dependence of the NICMOS non-linearity.

Chapter 2

Figure 2.1 Schematic for the original design plans for a precisely varying light source inside a cold DEWAR.

Figure 2.2 Existing DEWAR (blue) mated with new extension (gold). Light source and introductory optics not pictured.

Figure 2.3 Schematic of the DEWAR extension.

Figure 2.4 Left panel: NIR photodiode current vs. time for the current regulated lamp. Right panel: Infrared photodiode current vs. time for the lamp after the addition of the reference feedback photodiode.

Figure 2.5 Left panel: NIR photodiode current vs. temperature. Right panel: Visible photodiode current vs. temperature.

Figure 2.6 Left panel: NIR photodiode current vs. time. Right panel: Visible photodiode current vs. time.

Figure 2.7 The pattern emitted by the glass rod before the introduction of the diffusion paper.

Figure 2.8 Schematic of the components of the DEWAR extension and external optics.

Figure 2.9 Dark current vs. optical density (neutral density filter) for NIR and visible photodiodes on specific dates.

Figure 2.10 Current vs. time of the NIR photodiode.

Figure 2.11 Flux measurement of the detector vs. time.

Figure 2.12 Left panel: Flux of the detector vs. time with the incorrect read time. Right panel: Flux of the detector vs. time with the correct read time.

Figure 2.13 The flux of the detector vs. time.

Figure 2.14 Detector dark current vs. time.

Figure 2.15 Dark current vs. time of the detector and an exponential fit to the data.

Figure 2.16 The points are normalized detector to photodiode ratios vs. time and the lines are normalized detector readings vs. time.

Chapter 3

Figure 3.1 Current vs. optical density (neutral density filter) for photodiode dark measurements.
Figure 3.2 Current of useful photodiodes vs. current of reference photodiode.
Figure 3.3 Current vs. time for the NIR photodiode.
Table 3.1 Measured neutral density filter optical densities.
Figure 3.4 Residuals vs. optical density (neutral density filter) for the visible and NIR photodiodes.

Chapter 4

Figure 4.1 High illumination imgae of the detector with an area of uniform QE and minimal defects highlighted.
Figure 4.2 Top panel: Close up of the section selected in Figure 4.1. Bottom panel: The same figure after applying the mask.
Figure 4.3 Left panel: Detector to photodiode ratio vs. well fill of the detector. Right panel: Fractional reciprocity failure vs. well fill of the detector.
Figure 4.4 Left panel: Ratio of detector flux to NIR photodiode current vs. the NIR photodiode current. Right panel: Ratio of detector flux to visible photodiode current vs. the visible photodiode current.
Figure 4.5 Ratio of NIR to visible photodiode currents vs. NIR current.
Figure 4.6 Ratio of NIR to visible photodiode currents vs. NIR current after alterations and with the 790 nm laser.
Figure 4.7 Schematic of the components of the DEWAR extension and external optics for the laser setup.
Figure 4.8 Left panel: Photodiode current vs. optical density. A linear fit of the same slope is applied to each set. Right panel: The non-linearity from the linear fit to the data vs. photodiode current.
Figure 4.9 Left panel: Ratio of detector flux to NIR photodiode current vs. the NIR photodiode current. Right panel: Ratio of detector flux to visible photodiode current vs. the visible photodiode current.

Appendix A

Component, manufacturer and part number for the reciprocity setup.

Appendix B

Detailed Drawing of the DEWAR Extension

Appendix C

Extension Disassembly Procedure

Chapter 1

Overview

Dark Energy

At the end of the 20th century it was discovered that not only is our universe expanding, but its expansion is accelerating. Since this discovery there have been many independent corroborating sources to the accelerating expansion of the universe. There is no longer the question of whether it is accelerating or not, but it is a question of how large is the acceleration and what is causing it. The most popular hypothesis for causing this acceleration, dark energy, has since been on the minds of physicists and astronomers all over the world.

Dark energy can be explained by a variety of options: vacuum energy, quintessence, breakdown of General Relativity, higher dimensions, etc. Determining the nature of dark energy is an extremely difficult task. In order to do so a variety of observational techniques must be utilized, such as cosmic microwave background, baryon acoustic oscillations and late-time integrated Sachs-Wolfe effect, gravitational lensing and type Ia supernova. Type Ia supernova are extremely useful standard candles, being both extremely bright and consistently the same brightness. They are used as both observational devices themselves and as a distance measure in coherence with other experiments.

SNAP

The SuperNova Acceleration Probe (SNAP) project is a proposed space mission that is the catalyst for this research. It is a proposed space satellite that can measure the expansion of the Universe and characterize dark energy to a significantly greater accuracy than all preceding experiments. The proposed mission is expected to use 1.7 micron cut-off HgCdTe detectors for its observations and can sample over 2000 supernova up to a redshift of z=1.7; this can determine the expansion history of the universe over the last 10 billion years to an accuracy of 1% [1].

Precision Photometry

Precision photometry is essential to quantifying dark energy because it is necessary for all accurate distance measurements, at the few percent level, that extend over cosmic scales. For example, the inability to measure the peak brightness of a type Ia supernova to a few percent will not be accurate enough to constrain cosmological parameters to the required levels. Photometric redshifts are essential given that the wealth of data becoming available from large-scale sky surveys makes measuring distances utilizing

traditional spectroscopic methods unfeasible [3]. The attributes listed in Table 1.1 [4] must be measured and quantified in order for the precision photometry characterization of astronomical detectors.

• Detector Sensitivity --Gain --Read Noise --Dark Current --Quantum Efficiency --Well Depth	• Detector Uniformity --Inter-pixel Response Uniformity --Intra-pixel Response Uniformity --Reciprocity Failure --Lateral Charge Diffusion --Linearity in the Well
• Detector Stability --Latent Charge --Thermal Stability	• Detector Performance --Multiplexer Glow --Reset Behavior

Table 1.1: Attributes that must be characterized for precise photometry.

Precision Photometry at The University of Michigan

The University of Michigan is leading the way on precision photometry in its state-of-the-art NIR laboratory that is fully compliant with ESD (ElectroStatic Discharge) safety standards. Equipped to test virtually every aspect of precision photometry including groundbreaking measurements of Inter-pixel Response Uniformity [5], Intra-Pixel Response Uniformity [5], Quantum Efficiency [6] and linearity in the well [5] have been produced. The newest setup in the lab is a specially designed DEWAR that will quantify reciprocity failure.

Reciprocity Failure

Reciprocity failure is a count-rate dependent non-linearity in the detector. For example, a detector exposed to a source of 10,000 photons/second for 10 seconds will show a larger signal than if it is exposed to a source of 100,000 photons/second for 1 second.

The reciprocity failure of 2.5 micron cut-off HgCdTe detectors was originally documented by NICMOS 2005-002 [2] and is distinctly different from the well known total count dependent nonlinearity due to saturation as the well is filled. The nonlinearity on NICMOS, 5-6%/dex, shown in Figure 1.1 (right panel), exhibits a power law behavior, with pixels with high count rates detecting slightly more, and pixels with low count rates detecting slightly less flux than expected for a linear system [7]. Since this discovery, reciprocity failure calibration has become an important issue for all astronomical instruments, including SNAP.

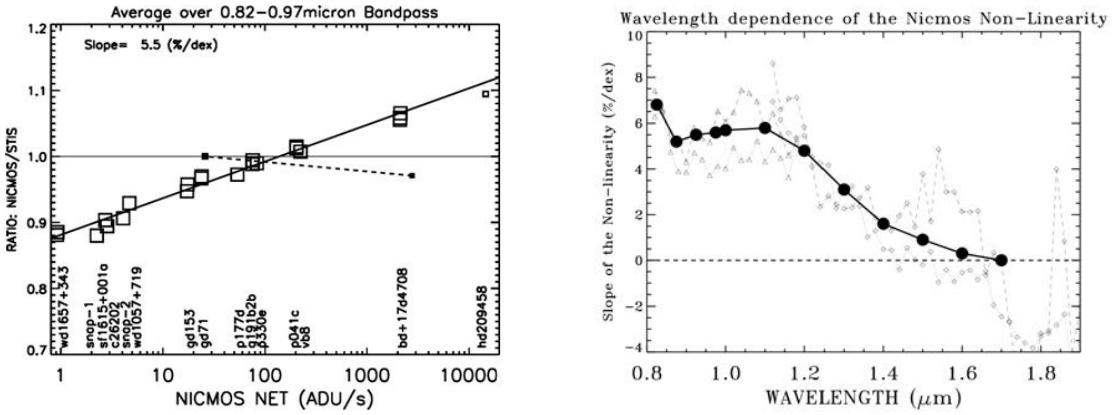

Figure 1.1: Left panel: NICMOS arrays (2.5 μm cut-off HgCdTe) on HST exhibit a 5-6%/dex flux dependent non-linearity. Right panel: The wavelength dependence of the NICMOS non-linearity.

The wavelength dependence of the nonlinearity of NICMOS is depicted in Figure 1.1 (right panel). Because we are using a 790 nm laser we would expect to find a reciprocity failure of 6-8%/dex.

The Detector and Photodiodes

The detector utilized in the experiment is a 1.7 micron cut-off HgCdTe photodetector purchased from Teledyne Scientific & Imaging under the product number H2RG SNAP-102. The effective area of the detector is 13.59 cm^2 consisting of a 2048×2048 grid of pixels each with an area of 324 μm^2.

The NIR photodiode used in the experiment was purchased from Hamamatsu Photonics under the product number G10899-01K. It is an InGaAs PIN photodiode with an effective area of 0.785 mm^2 and a spectral response between 0.5 μm and 1.7 μm. The visible photodiode was purchased from Edmund Optics under the product number 53371. It is a silicon photodiode with an effective area of 5.1 mm^2 and a spectral response between 0.5 μm and 1.1 μm.

Chapter 2

Experimental Setup

The problem presented was to design a system with a uniform and precisely varying near infrared (NIR) light source in an environment with cryogenic temperatures and vacuum up to 10^{-8} mBar. Reciprocity failure is also important to visible detectors, such as CCDs, so all of the optics in our design should be compatible with the visible spectrum.

Original Design

Initially our design was intended to utilize the well know intensity difference, $1/r^2$, of a point source as its distance to the detector is varied. Figure 2.1 is a schematic for the proposed design.

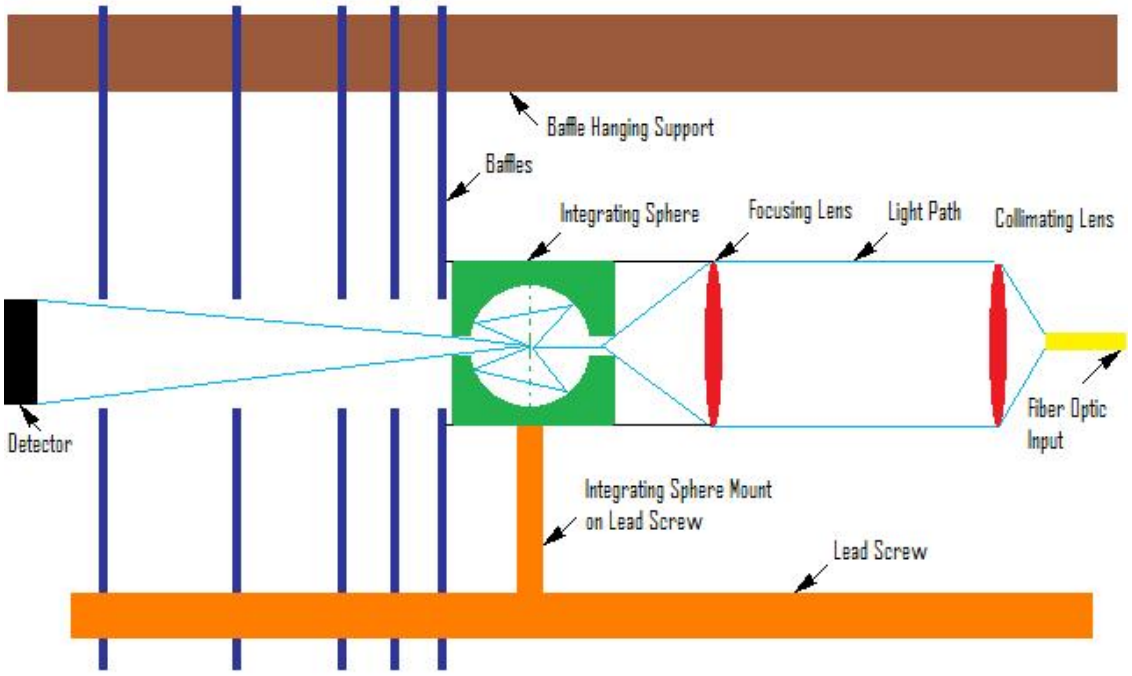

Figure 2.1: Schematic for the original design plans for a precisely varying light source inside a cold DEWAR.

The light path, as shown by the schematic, originates at the fiber optic input. The light is then collimated by a lens which remains stationary with respect to the fiber optic input at all times. This collimated light then travels a variable distance before it is incident on the collimating lens. This lens, which remains stationary with respect to the integrating

sphere, focuses the light into the integrating sphere. The integrating sphere then releases the light towards the detector, where any stray light is blocked by the baffles. The baffles are hanging from the 'baffle support' and are linked together and to the integrating sphere, as to perform like an accordion, stretching to a specific length as the integrating sphere moves away from the detector, and collapsing on top of one another as the integrating sphere approaches the detector. The lead screw at the bottom is attached to the integrating sphere as to provide an accurate measurement of the distance between the detector and the integrating sphere.

The complexities of this design are numerous and difficult to overcome. The design requires precision optics, independent of wavelength and temperature, which can be subjected to cryogenic temperatures. In addition a moveable baffle system in the cold that must not bind or snag must be designed. In order to generate a light source that varies over 5 orders of magnitude the available distance to travel must be very large, requiring a long DEWAR extension (minimum 1 meter) that can still be cooled appropriately. These difficulties are too large and too many for this to be a practical solution.

Actual Design

A more practical approach is to utilize apertures to create a precisely varying light source that is independent of wavelength and dependent only on the geometry (size) of the aperture. An extension is still required but a much shorter one will suffice and the new design has many less moving parts. The original DEWAR (blue) and extension (gold) are shown in Figure 2.2.

Figure 2.2: Existing DEWAR (blue) mated with new extension (gold). Light source and introductory optics not pictured.

The path of illumination through the extension is as follows in the schematic in Figure 2.3. The specific parts and product numbers, a detailed drawing of the DEWAR extension and the disassembly procedure can be found in appendix A, B and C, respectively.

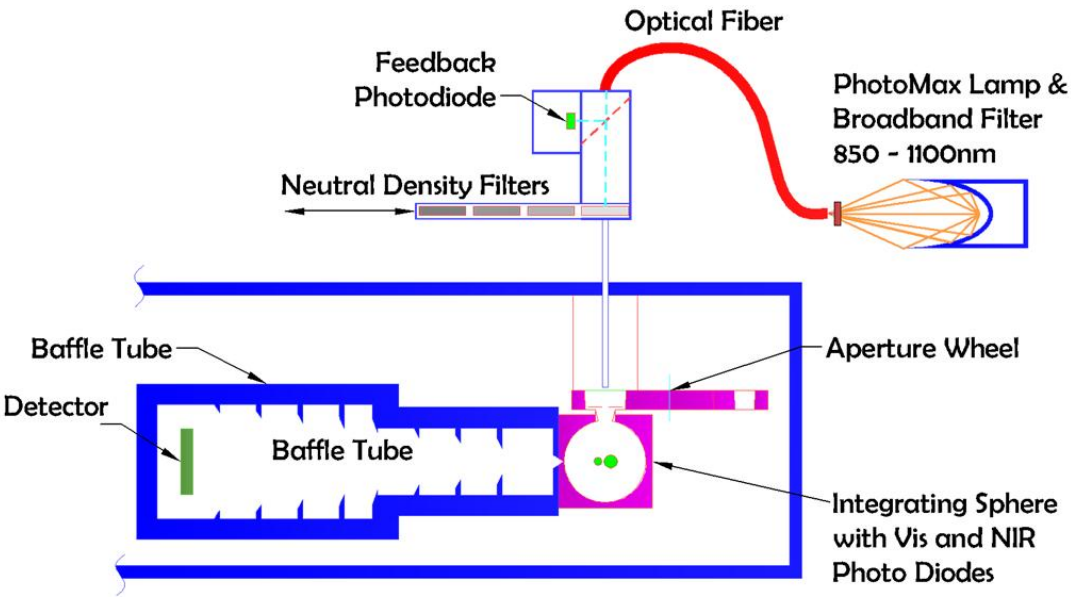

Figure 2.3: Schematic of the DEWAR extension.

A 50 W Quartz-Tungsten-Halogen lamp illuminates a fiber optic after passing through an 850-100 nm broadband filter. This light then passes an intensity feedback controller that stabilizes the light intensity. The last step before entering the system is that the light passes through the selected neutral density filter (one of four). The remaining intensity is focused into an optical fiber (a glass rod) which enters into the DEWAR extension. The light travels the length of the glass rod and is incident on the selected aperture in the aperture wheel (one of eight). Apertures 2 through 7 range from 10µm to 3.3mm, allowing a dynamic range of approximately 10^5,while aperture 1 is a blank and aperture 8 has a full opening in the wheel with no aperture. The light that passes through the aperture is introduced into the integrating sphere. One of the ports on the sphere houses two reference photodiodes. The other opens into the baffle tube in the direction of the detector. The circular baffles block any reflected light.

This design eliminates many of the problems that occur in systems in which the instruments are located outside of the DEWAR. The instruments are enclosed so there is no interaction with the temperature, humidity or lighting of the room. In addition there is no entrance window which eliminates issues of reflections, distortions and emitting in the NIR. With this design the ratio of flux incident on the detector and flux incident on the photodiodes remains constant.

Encountered Difficulties

External Factors

With the vacuum pump in three different states, running, slowing down and completely off, we monitored the photodiode and detector readouts. The effects of the vacuum pump are small enough as to have no effect on the photodiode or detector readouts.

The signal to noise ratio of the photodiode readouts was significantly improved by: shortening the length of the cables, providing better cable shielding, providing each photodiode with its own picoammeter, and properly grounding each of the photodiodes.

We must replenish the liquid nitrogen every eight hours in order to maintain the cryogenic temperature inside the DEWAR. The refilling of the DEWAR affects the photodiode and detector readouts and subsequently the means by which we take reciprocity measurements. Currently all of our measurements are taken within a single eight hour period of time so the liquid nitrogen filling does not interfere with our results.

Pixel self heating is characterized by temperature changes at the 'pixel level' caused by an interruption in the clocking cadence of the detector. Continuously clocking the detector eliminates this effect [5].

Lamp Stability

Regulating the voltage in order to control the lamp leads to an extremely unstable light source. Using the current regulation mode of the lamp produced illumination stable to within 1.0%, see Figure 2.4 (left panel), which is inadequate for our purposes. We then installed a reference feedback photodiode and the light source became stable to less than 0.5%, see Figure 2.4 (right panel).

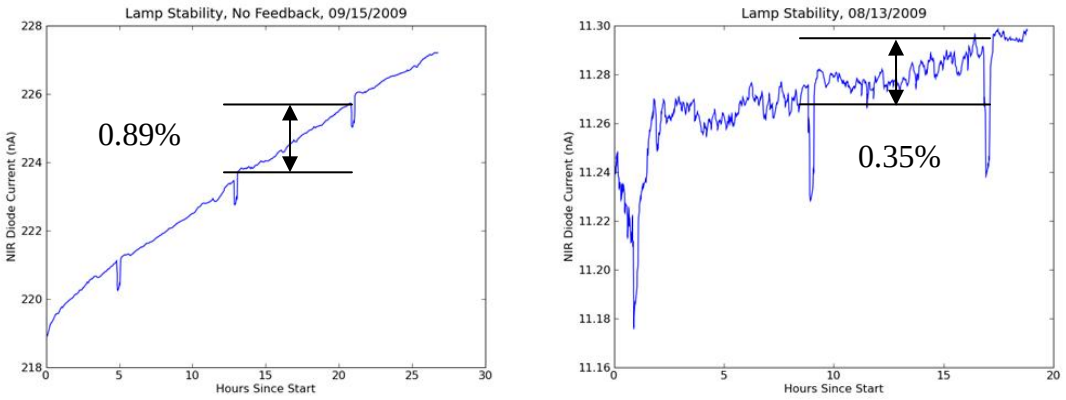

Figure 2.4: Left panel: NIR photodiode current vs. time for the current regulated lamp. Right panel: Infrared photodiode current vs. time for the lamp after the addition of the reference feedback photodiode.

Photodiode Stability

The quantum efficiency of the photodiodes is temperature dependent. On 11-07-09 using the 790 nm laser, no feedback photodiode and no bandpass filter we measured the temperature dependence for each photodiode to be less than 0.1%/K and is depicted in Figure 2.5. This temperature dependence is negligible because the photodiodes are temperature controlled to 10 mK.

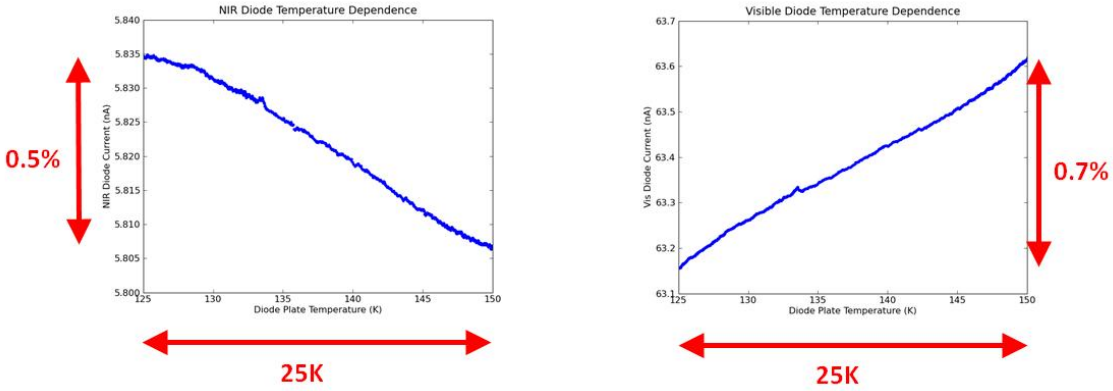

Figure 2.5: Left panel: NIR photodiode current vs. temperature. Right panel: Visible photodiode current vs. temperature.

Laser Stability

The laser proved to be stable to 2.4% as depicted in Figure 2.6. The flux from the laser changes somewhat over long periods of time but we monitor this change in real time with the photodiode currents to correct for the drift.

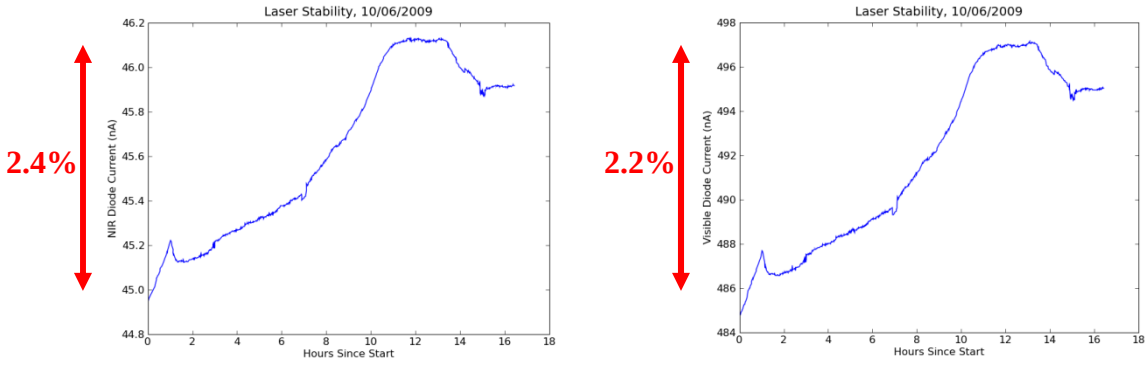

Figure 2.6: Left panel: NIR photodiode current vs. time. Right panel: Visible photodiode current vs. time.

Non-Reproducible Apertures

The problem with aperture reproducibility was that we assumed the optical fiber (glass rod) was emitting a flat image. Upon close investigation the pattern in Figure 2.7 is what was actually produced. We found placing a thin layer of diffuse material immediately after the glass rod visibly eliminates the pattern.

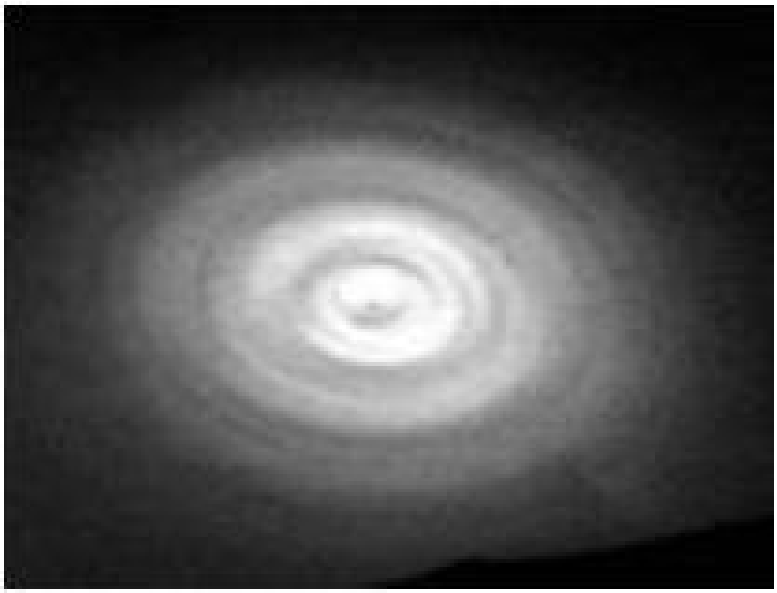

Figure 2.7: The pattern emitted by the glass rod before the introduction of the diffusion paper.

Non-Reproducible Neutral Density Filters

As the filters were moved into and out of position there was mechanical movement of the entire filter assembly causing reproducibility to only 7%. Clamping the filter changer more securely to the DEWAR extension made the filters reproducible to within 0.5%.

Light Leaks

Direct sunlight affected the readouts of the photodiode and detector. We installed port covers attached to the cold shield of the DEWAR and extended the baffle tube to encompass the detector, see Figure 2.8. Intense sunlight still produced an effect so we installed a thick black sheet; covering the only nearby window and eliminating any direct sunlight.

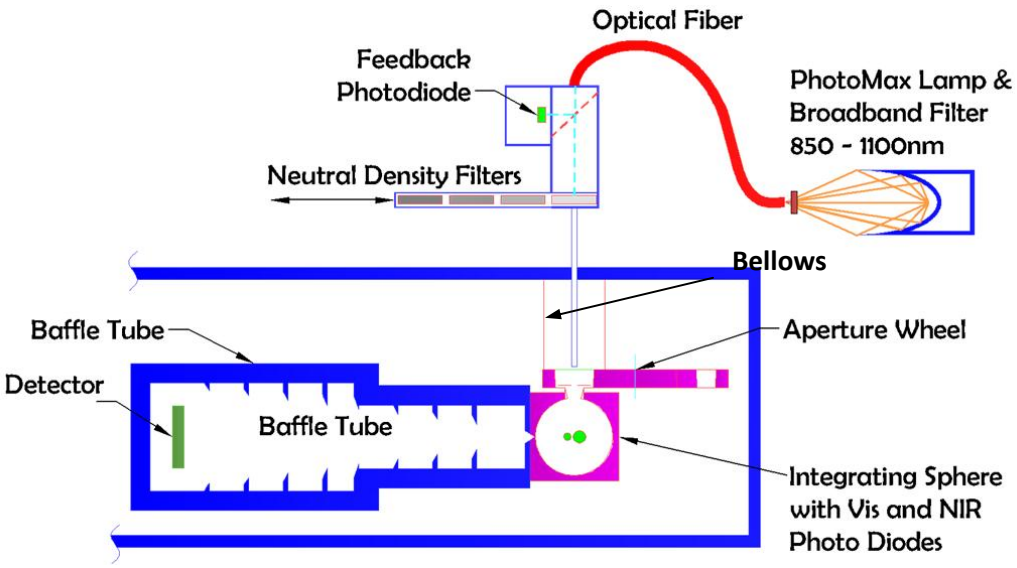

Figure 2.8: Schematic of the components of the DEWAR extension and external optics.

Aperture Heating (Fake Light Leaks)

Initially the NIR photodiode and the visible photodiode displayed different characteristics with respect to increasing the optical density (neutral density filter). A measure of the dark current vs. incident flux is shown in Figure 2.9. The earlier readings were taken when the apparatus only housed one photodiode on the integrating sphere and indicates a different recorded dark current based on whether it was a visible or NIR photodiode. Once we noticed this problem, we altered the photodiode mount on the integrating sphere to house both a visible and NIR photodiode at the same time. In addition the apertures, with gold on one side and black on the other, were flipped to orient the gold side upwards, increasing the reflectance of the apertures and eliminating the effect of aperture heating. This is visible in the complete overlap of dark currents measured on 04-07-2009 in Figure 2.9.

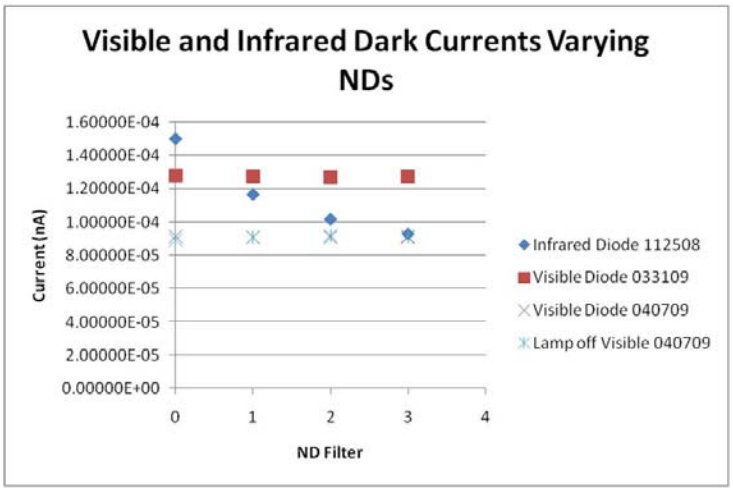

Figure 2.9: Dark current vs. optical density (neutral density filter) for NIR and visible photodiodes on specific dates.

Persistence

Persistence is a memory effect in which collected charge from a previous measurement temporarily increases the reading of the following measurement. In Figure 2.10 the current of the NIR photodiode decreases to the expected dark reading seconds after the incident flux is reduced to zero. This indicates the NIR photodiode has no persistence.

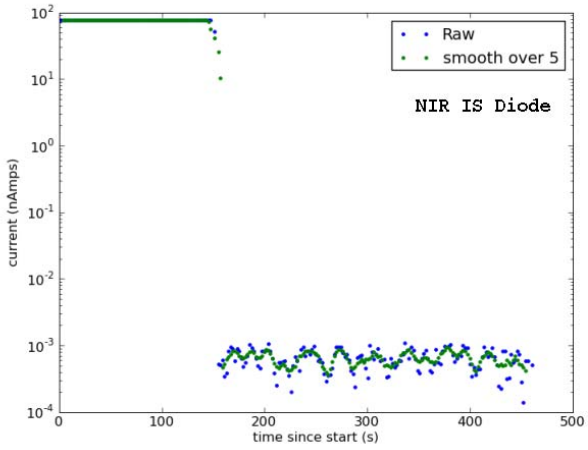

Figure 2.10: Current vs. time of the NIR photodiode.

Figure 2.11 is a measurement of the detector at a very low flux, thirty seconds after a 60% well fill of the detector. The deviation from linearity in the beginning seconds of the plot is evidence of persistence in the detector.

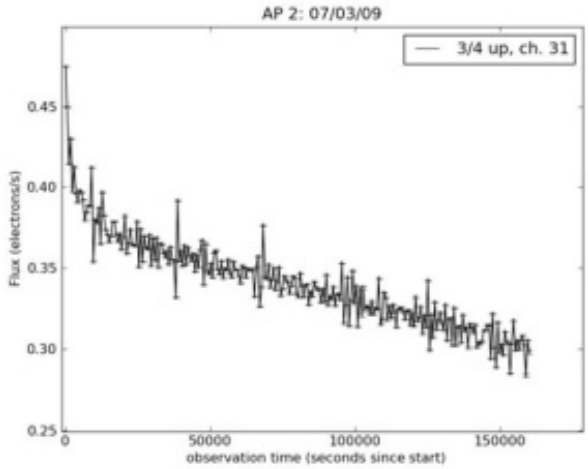

Figure 2.11: Flux measurement of the detector vs. time.

High flux images of the detector have enough intensity that persistence is negligible. Low flux images are generally taken after other low flux images (small well fill) so persistence is again negligible. Persistence decays with time so a low flux image can be taken after a high flux image after waiting an hour at most, based on the previous well fill of the detector.

Ambient Temperature

The photodiode electronics exhibited a temperature dependence that was not affecting the detector. Our solution to this was to implement a photodiode in the system that would be intentionally blocked from the light (by several layers of aluminum foil). While this photodiode is not affected by any light introduced into the system it still experiences the ambient temperature dependence which can subsequently be subtracted. The explanation of this procedure is outlined in the data section.

Exposure Timing Issues

The exposure time of the detector is the time between frames added to the read time. Figure 2.12 (left panel) indicates a dependence of detector flux based on the exposure time. The problem was that we did not know the read time accurately enough. Once we accurately measured the read time the detector readout no longer indicated a dependence on the exposure time, see Figure 2.12 (right panel).

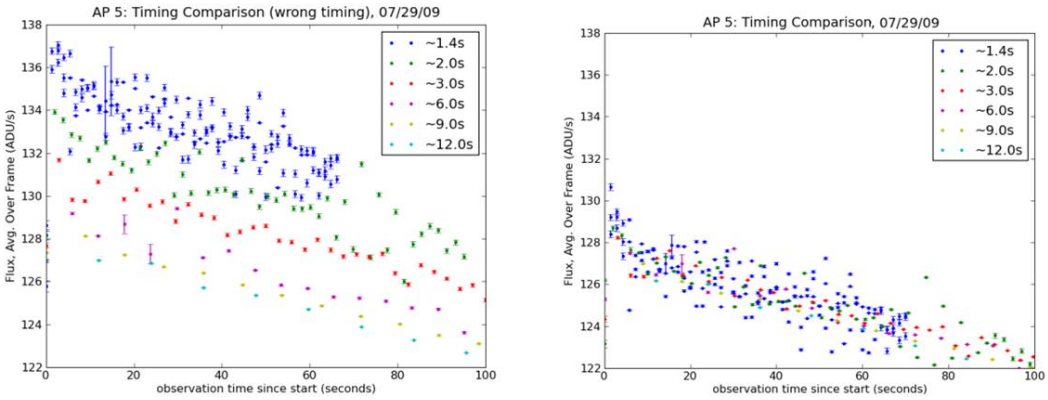

Figure 2.12: Left panel: Flux of the detector vs. time with the incorrect read time. Right panel: Flux of the detector vs. time with the correct read time.

Initial Spike in Images

The readout of the detector consistently has a deviation from expectation in the initial image of the readout, as seen in Figure 2.13.

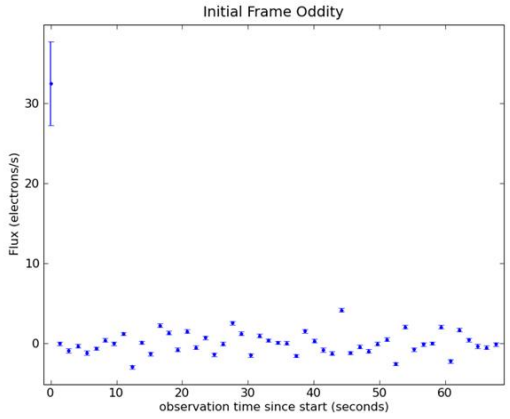

Figure 2.13: The flux of the detector vs. time.

We are still not sure what is causing this discrepancy in flux, but we believe it may be related to the edge glow where the electronics are connected to the detector. There are two reasons we do not need to quantify this discrepancy. It is only noticeable at very low flux images and because we record frames separately and subtract them from the preceding frame, as outlined in the data section, we can simply ignore these initial frames (same method as subtracting liquid nitrogen fills).

Detector Dark Current

We discovered, as you can see in Figure 2.14, that the detector has a higher dark current after it is turned on, which is decreasing in time. Thus for our measurements the detector has been running for at least 45 hours before data is taken.

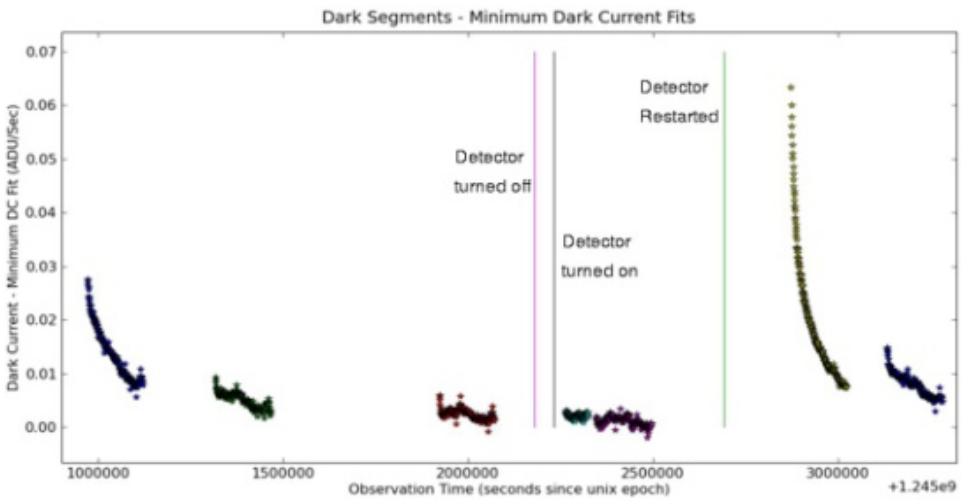

Figure 2.14: Detector dark current vs. time.

Reset Induced Dark Current

There is an exponential dark current decay after each reset of the detector, see Figure 2.15. We must reset the detector before each exposure so we have quantified this exponential decay of the dark current. After each reciprocity measurement there are dark measurements taken over the same time of day and exposure sequence. We then subtract the dark measurement in two different ways. The first being the calculation of the exponential fit as in Figure 2.15, and the second being a frame by frame subtraction.

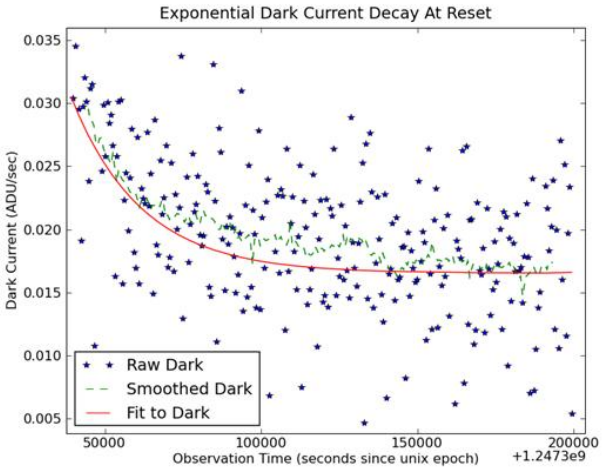

Figure 2.15: Dark current vs. time of the detector and an exponential fit to the data.

Long Term Drifts of Detector to Photodiode Ratios

The ratio of the detector to the photodiode should be independent of the flux of the system. Figure 2.16 indicates that in fact this ratio is not reproducible to less than 2%. The long term drifts of the detector to photodiode ratio are plotted in Figure 2.16 as points while the detector alone is plotted as lines. Sets 2 and 3 were taken 1 hour 25 minutes apart, five days after set 1.

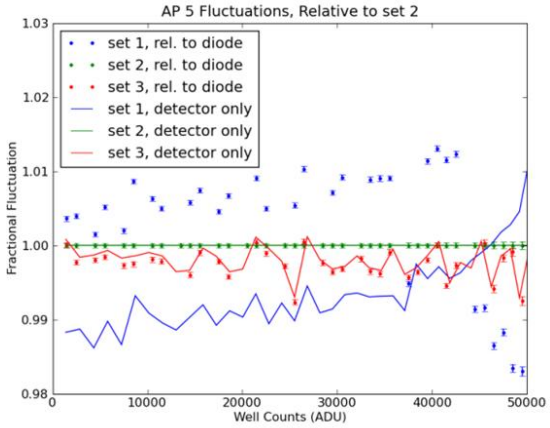

Figure 2.16: The points are normalized detector to photodiode ratios vs. time and the lines are normalized detector readings vs. time.

The correlation between the points and the lines indicates that the issue is detector dependent. Currently we are not sure the reason behind this deviation but believe it to be bias voltage drifts, detector temperature drifts (unlikely) or the temperature drift of the external electronics. These drifts are avoided by taking data over short periods of time or we can average them away with multiple samples, assuming these drifts are statistical over a very long time.

Chapter 3

Photodiode Calibration

Procedure

For measuring the photodiode linearity each aperture was maintained constant while the neutral density filters were varied from 0 to 3. We then took a dark measurement before proceeding to the next aperture. This is because the precise flux through an aperture is not reproducible after changing aperture but the flux through the neutral density filters, as they are changed, are reproducible to less than 0.5%. This is not an issue in characterizing the detector because only the ratio of the flux of the photodiode and detector is important, which is independent of the actual amount of light incident.

The most vital part of this measurement is accurate and reproducible dark measurements. Aperture 1 is a 'blank' in the system. When it is selected, there should be no flux through the system. We indicate this is the case by comparing dark measurements with aperture 1 and all four neutral density filters. Any light leaks or failure of the blank would be evident in a change in flux with respect to neutral density filter, as seen in Figure 2.9. There are no light leaks as Figure 3.1 indicates.

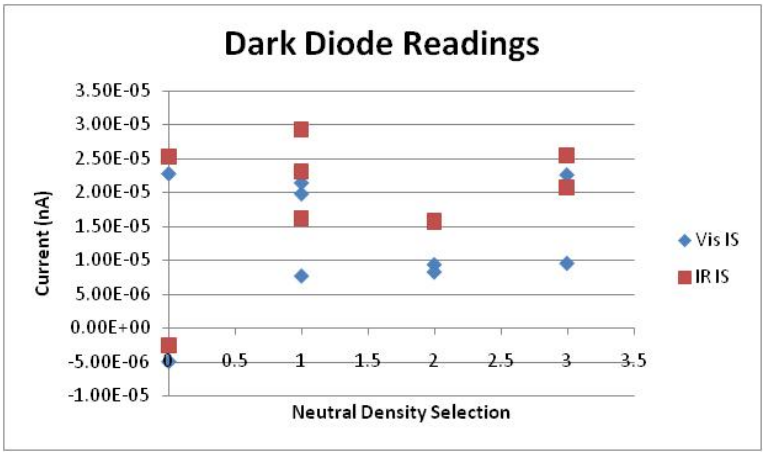

Figure 3.1: Current vs. optical density (neutral density filter) for photodiode dark measurements.

Data Analysis

The photodiode data during and adjacent to liquid nitrogen fills are compromised, as demonstrated in Figure 2.4. To account for this our linearity measurements are taken over one eight hour period, between liquid nitrogen fills, eliminating the issue.

In order to correct for the temperature dependence a linear fit of the reference current to the useful current gives the useful photodiode value as a function of the reference photodiode value, see Figure 3.2. So when light is introduced, the fit gives the value of the useful photodiode as if it was dark.

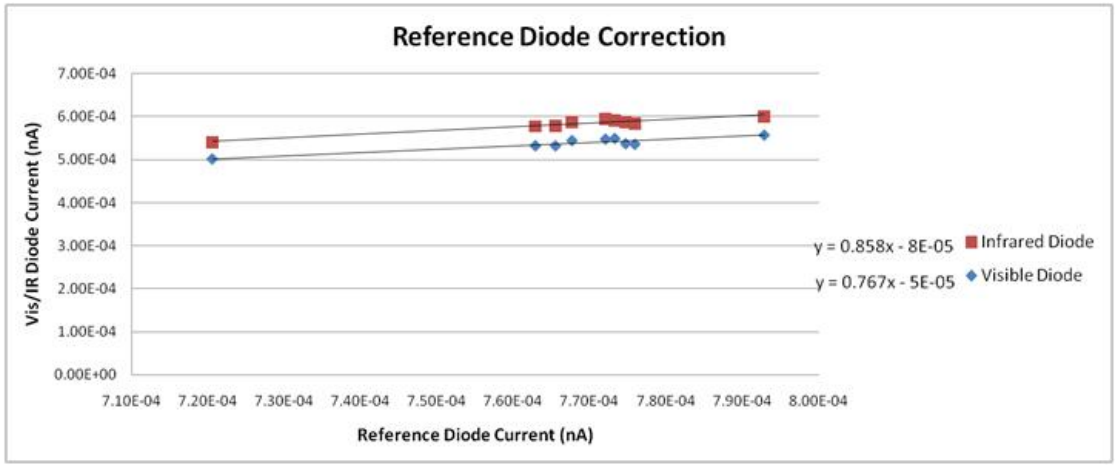

Figure 3.2: Current of useful photodiodes vs. current of reference photodiode.

As shown in Figure 3.3 using this reference photodiode greatly improves the values and stability of the photodiode readings.

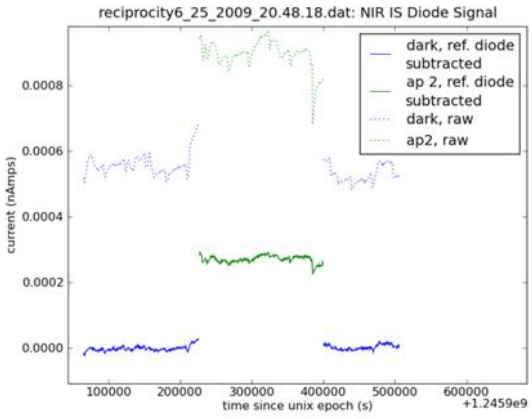

Figure 3.3: Current vs. time for the NIR photodiode.

We then calibrated the optical density of each neutral density filter, see Table 3.1. The logarithm of the flux of no neutral density filter (ND0) over each neutral density filter

(ND1-3) results in the optical density of that neutral density filter (i.e. $\log(F_{ND0}/F_{ND2})=2.04$) . Large errors at the lower light levels limited our calculation to apertures 5, 6 and 7. The fractional transmittance of a neutral density filter with optical density d is given by 10^{-d}, and is normalized to the d=0 value (ND0).

Optical Density		
	NIR	Visible
ND0	0	0
ND1	1.04	1.05
ND2	2.04	2.06
ND3	2.87	2.91

Table 3.1: Measured neutral density filter optical densities.

The next step in calculating the linearity is to plot the logarithm of the measured flux against the actual optical density of the filters. We then compare the linear fit of the data, using the same slope for each fit, to the measured values and find that the residuals all lie within ±0.8%, as shown in Figure 3.4.

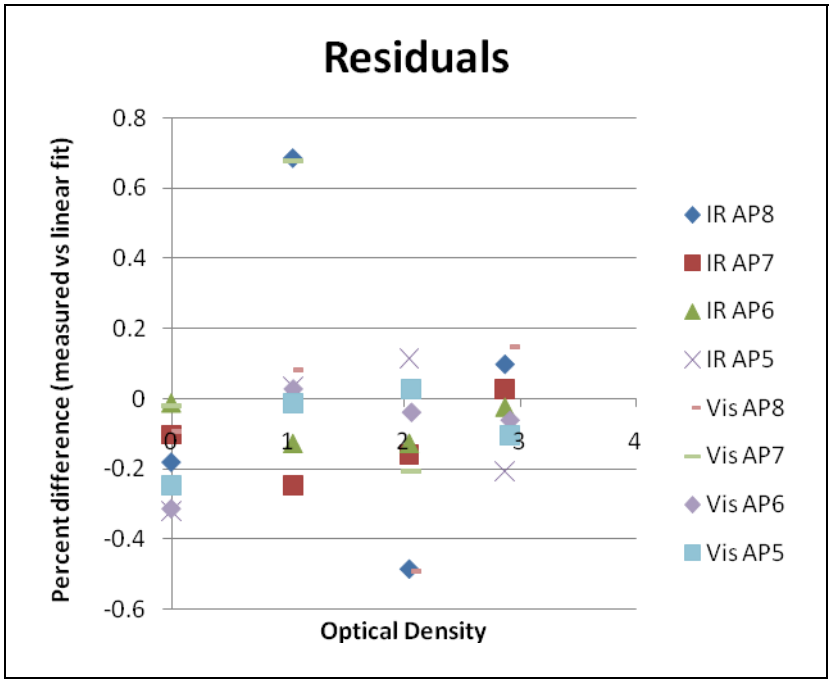

Figure 3.4: Residuals vs. optical density (neutral density filter) for the visible and NIR photodiodes.

Conclusion

On 04-10-09 with the 50 W QTH lamp, the 800-1150 nm bandpass filter, the NIR photodiode, and a 900 micron aperture in place before the feedback photodiode we measured the photodiodes to be linear to within 1% over five orders of magnitude and only at very low light levels does the linearity deviate. Thus we can use the precise linearity of the photodiodes in accordance with the detector in order to quantify reciprocity failure to less than a percent.

Chapter 4

Detector Reciprocity

Procedure

Reciprocity failure occurs when similarly filled wells, the same integrated intensity, with different incident fluxes result in a differing capture of electrons. In order to quantify this we filled the well of the detector to 60% of the full well using a dynamic range of five orders of magnitude in intensity. To increase the readout speed we selected a 300 row region of the detector that also had uniform quantum efficiency (QE) and minimal defects, see Figure 4.1.

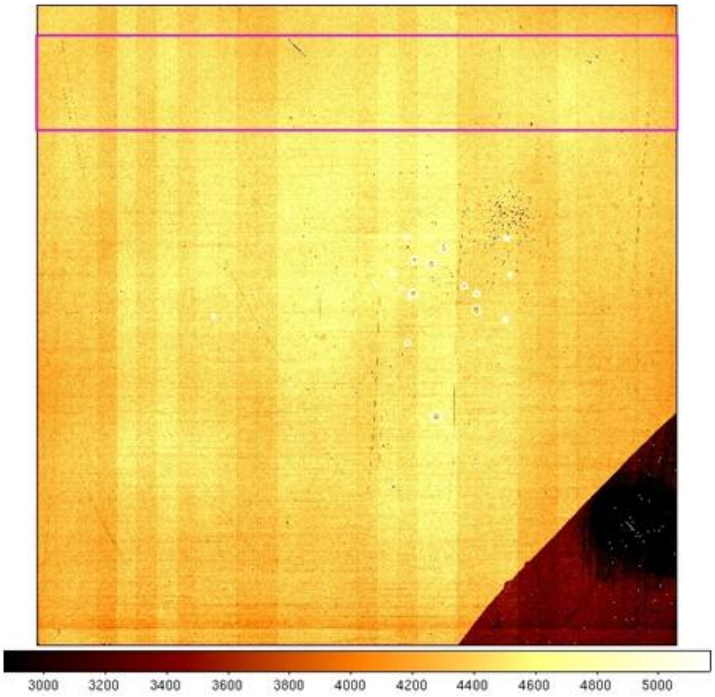

Figure 4.1: High illumination image of the detector with an area of uniform QE and minimal defects highlighted.

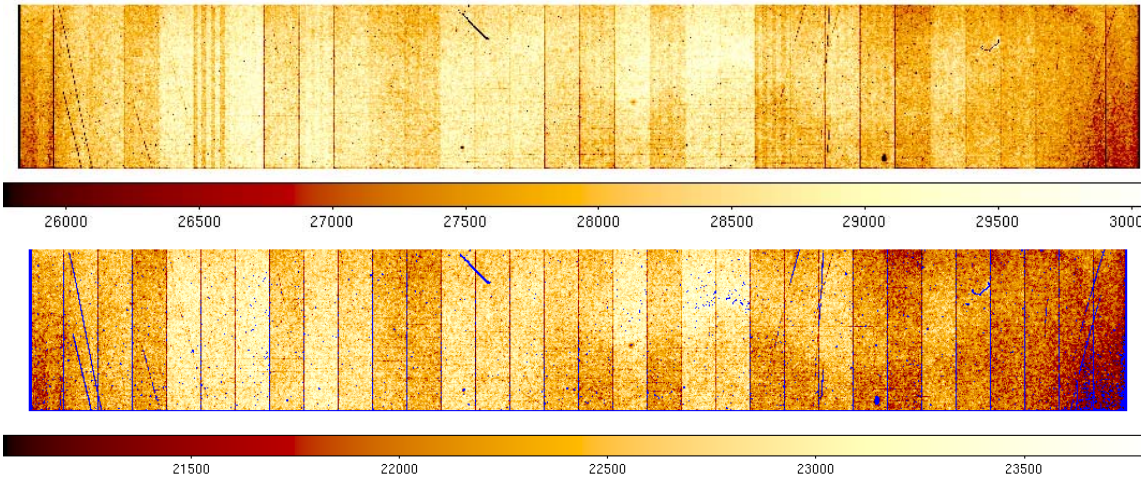

Figure 4.2: Top panel: Close up of the section selected in Figure 4.1. Bottom panel: The same figure after applying the mask.

We masked the bad pixels, shown in Figure 4.2, and averaged the remaining good pixels in each of the 32 channels. This value is then divided by the NIR photodiode. We then compared integrated intensities against the well fill of the detector to observe reciprocity failure.

Data Analysis

Our mask in Figure 4.2 is selected as pixels with much higher and lower counts than expected. Also any pixels adjacent to these and any adjacent to those are given an automatic value of NAN and are ignored for the remainder of the calculations. This results in masking 4% of the pixels in this region.

During liquid nitrogen fills there is noise introduced to both the detector and photodiodes. We compensate for that by 'clipping' the frames during and directly around fills. Our 'up-the-ramp' exposure quantifies the amount of charge accumulated between each frame (with hundreds of frames per exposure) thus we can ignore the frames affected by the nitrogen fills and continue utilizing the data that is accumulated after the fill. This is the same method we use when clipping the problematic initial image.

Conclusion

Between 06-25-09 and 07-22-09 with the 50 W QTH lamp, the 800-1150 nm bandpass filter, the NIR photodiode, and a 900 micron aperture in place before the feedback photodiode we calculated an upper limit on reciprocity of the H2RG SNAP-102 device to be within 2% over three orders of magnitude, as depicted in Figure 4.3.

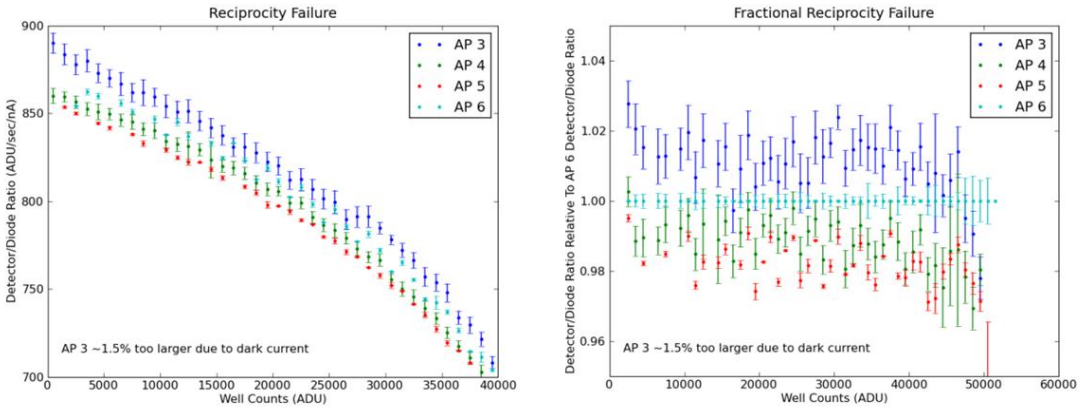

Figure 4.3: Left panel: Detector to photodiode ratio vs. well fill of the detector. Right panel: Fractional reciprocity failure vs. well fill of the detector.

Conclusion 2

On 09-11-09 with the 50 W QTH lamp, the 850-1100nm bandpass filter, and the NIR photodiode we calculated a reciprocity failure of -1.2%/dex over four orders of magnitude, see Figure 4.4 (left panel). This is smaller than that of NICMOS and it is negative. Using the visible photodiode the reciprocity failure is -2.0%/dex, and is again negative, see Figure 4.4 (right panel). These findings are different than that found with NICMOS. In addition this reveals that there is an NIR to visible current ratio that is not equal to 1, see Figure 4.5.

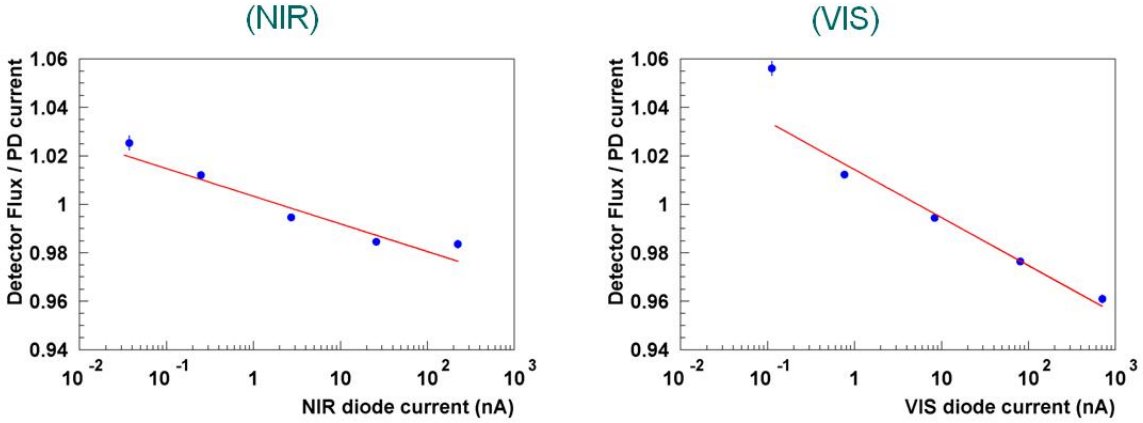

Figure 4.4: Left panel: Ratio of detector flux to NIR photodiode current vs. the NIR photodiode current. Right panel: Ratio of detector flux to visible photodiode current vs. the visible photodiode current.

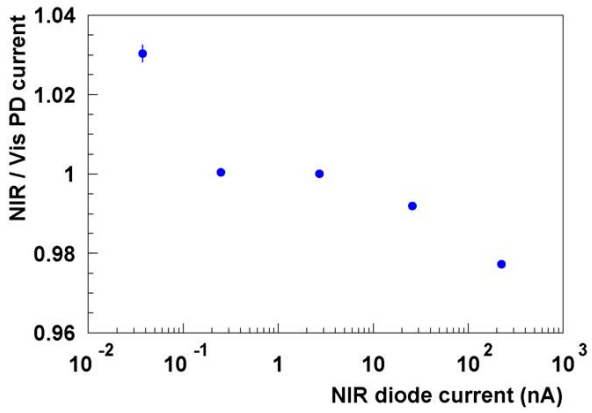

Figure 4.5: Ratio of NIR to visible photodiode currents vs. NIR current.

Laser Reciprocity Procedure

As conclusion 2 revealed, the NIR and visible photodiode current ratio is -1.3%/dex. Switching the physical location of the photodiodes, looking for a geometrical effect, did not alter the ratio. A 1" diameter 50 nm filter did not alter the ratio. Setting the photodiodes an inch back from the integrating sphere improved the ratio slightly. Replacing the visible photodiode with another NIR photodiode, looking for a spectral effect, improved the ratio slightly. A 0.5" diameter 50 nm filter improved the ratio slightly.

In order to remove many of the uncertainties involved in the system, we decided to make a reciprocity measurement utilizing a narrow band laser. The laser produces a large intensity at (790±1)nm. With the laser the NIR to visible photodiode current ratio improves to 0.4%/dex, see Figure 4.6.

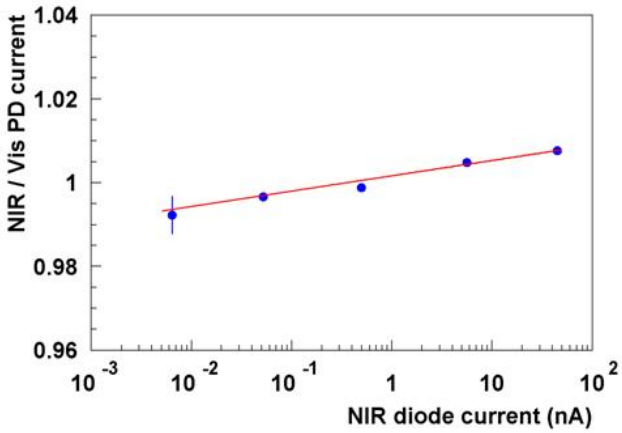

Figure 4.6: Ratio of NIR to visible photodiode currents vs. NIR current after alterations and with the 790 nm laser.

A schematic of the experimental setup involving the laser is depicted in Figure 4.7. It is identical to that earlier described except that the bandpass filter before the liquid light guide has been removed and the feedback photodiode is no longer being used.

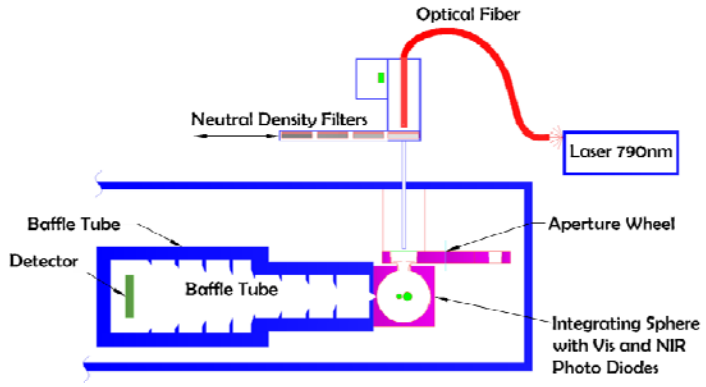

Figure 4.7: Schematic of the components of the DEWAR extension and external optics for the laser setup.

The photodiode linearity was calculated utilizing the same method described earlier. The laser was found to be linear to less than ±0.5% over five orders of magnitude in flux, see Figure 4.8.

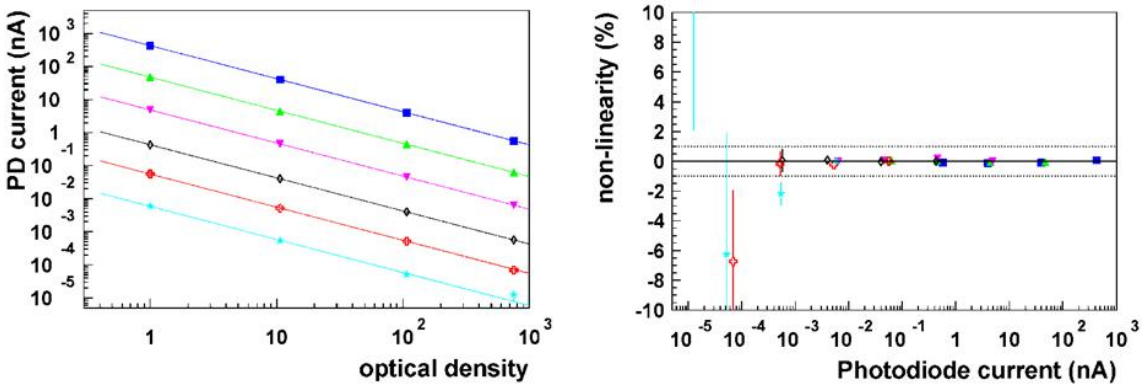

Figure 4.8: Left panel: Photodiode current vs. optical density. A linear fit of the same slope is applied to each set. Right panel: The non-linearity from the linear fit to the data vs. photodiode current.

Laser Reciprocity Conclusion

On 09-10-09 with the 790 nm laser, no bandpass filter, and the NIR photodiode we calculated a reciprocity failure of (-0.23±0.1)%/dex over four orders of magnitude, see Figure 4.9 (left panel). This is again smaller than that of NICMOS and it is negative. Using the visible photodiode the reciprocity is (0.091±0.097)%/dex, and is now positive, see Figure 4.9 (right panel). These findings indicate a reciprocity failure of less than ±0.25%/dex for the H2RG SNAP-102 detector.

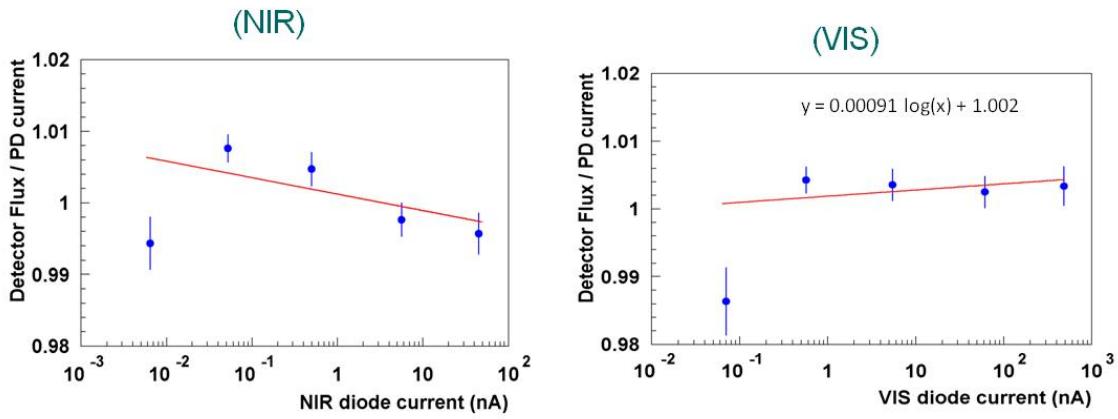

Figure 4.9: Left panel: Left panel: Ratio of detector flux to NIR photodiode current vs. the NIR photodiode current. Right panel: Ratio of detector flux to visible photodiode current vs. the visible photodiode current.

Summary

Achieving precision photometry is a daunting task, but as more precise measurements are required, performance specifications of detectors increase dramatically. Among the required performance specifications is detector linearity at the below 1% level. To achieve this high level of detector linearity reciprocity failure must be carefully studied and characterized. NICMOS originally documented reciprocity failure to be a 5-6%/dex nonlinearity, with a larger integrated signal corresponding to a larger flux. With our dedicated experimental setup for the characterization of reciprocity failure we illustrated that the reciprocity failure of the H2RG SNAP-102 1.7 micron cut-off HgCdTe photodetector at 790nm is less than ±0.25%/dex.

This work was supported by DOE grant No. DE-FG02-08ER41566.

References

[1] SNAP Collaboration, 'SuperNova Acceleration Probe (SNAP),' <http://snap.lbl.gov>

[2] R.S. de Jong, et al., "NICMOS status", *arXiv:0604394 [astro-ph]* (April 2006)

[3] M. Banerji, F. B. Abdalla, O. Lahav, and H. Lin, "Photometric Redshifts for DES and VISTA and Implications for Large Scale Structure", *arXiv:0711.1059v1 [astro-ph]* (November 2007)

[4] Karabina, Anastasia, "Characterizing the Absolute Quantum Efficiency of SNAP NIR Photodetectors", Honors Thesis, University of Michigan, (2008)

[5] M. G. Brown, "Development of NIR Detectors and Science Requirements for SNAP", Ph.D. Thesis, University of Michigan, (2006)

[6] M. Schubnell, M. G. Brown, A. Karabina, W. Lorenzon, N. Mostek, S. Mufson, G. Tarle, C. Weaverdyck, "Precision Quantum Efficiency Measurements on 1.7 Micron Near Infrared Devices", SPIE, Volume 7021, (2008)

[7] W. Lorenzon, and M. Schubnell, "Precision Photometry to Study the Nature of Dark Energy"

Appendix A

	Component	Manufacturer	Part Number
	DEWAR	IRLabs	ND-8 #3715
	DEWAR Estension	IRLabs	UMCHRK15S
	Power Supply	Newport	69931
	Photomax Housing	Newport	60100
	Interface Plate Assembly	Newport	60925
	50W QTH Lamp	Newport	6332
	Ellipsoidal Reflector	Newport	60113
	Pyrex Window	Newport	60127
	3 IN Flange Double Female	Newport	66291
	Light Shield	Newport	71381
	Bandpass Filter (720-2500)	Edmund Optics	54754
	Bandpass Filter (850-1100)	Omega Optical	3RD850-1100
	3-1 ½ IN Step Down Adaptor	Newport	66290
	Fiber Bundle Holder	Newport	77802
	Liquid light guide	Newport	77634
	Light Intensity Controller	Newport	68950
	Neutral Density 1 (700-1100)	Edmund Optics	47530
	Neutral Density 2 (700-1100)	Edmund Optics	47533
	Neutral Density 3 (700-1100)	Edmund Optics	47535
	Quartz Glass Rod (3mm ø)	SNAP Lab	-------
	Vacuum Feedthrough	Swagelok	SS-2-UT-A-6
	Feedthrough Baffle	SNAP Lab	-------
	Aperture Wheel	IRLabs	
	Apertures	Lenox Laser	HP-3/8-DISC-AU
	Integrating Sphere	SphereOptics	SPH-2Z-4
	Visible Photodiode (Large)	Edmund Optics	54035
	Visible Photodiode (Small)	Edmund Optics	53371
	2 NIR Photodiodes	Hamamatsu	G10899-01K
	4 Picoammeters (Diode Readouts)	Keithley	6485
	Detector	Teledyne	H2RG SNAP-102
	Leech Electronics (Detector Readout)	Leech	
	Laser (790±1)	OPTO Power Corp.	OPC-A015-FCPS

Table A.1: Component, manufacturer and part number for the reciprocity setup.

Appendix B

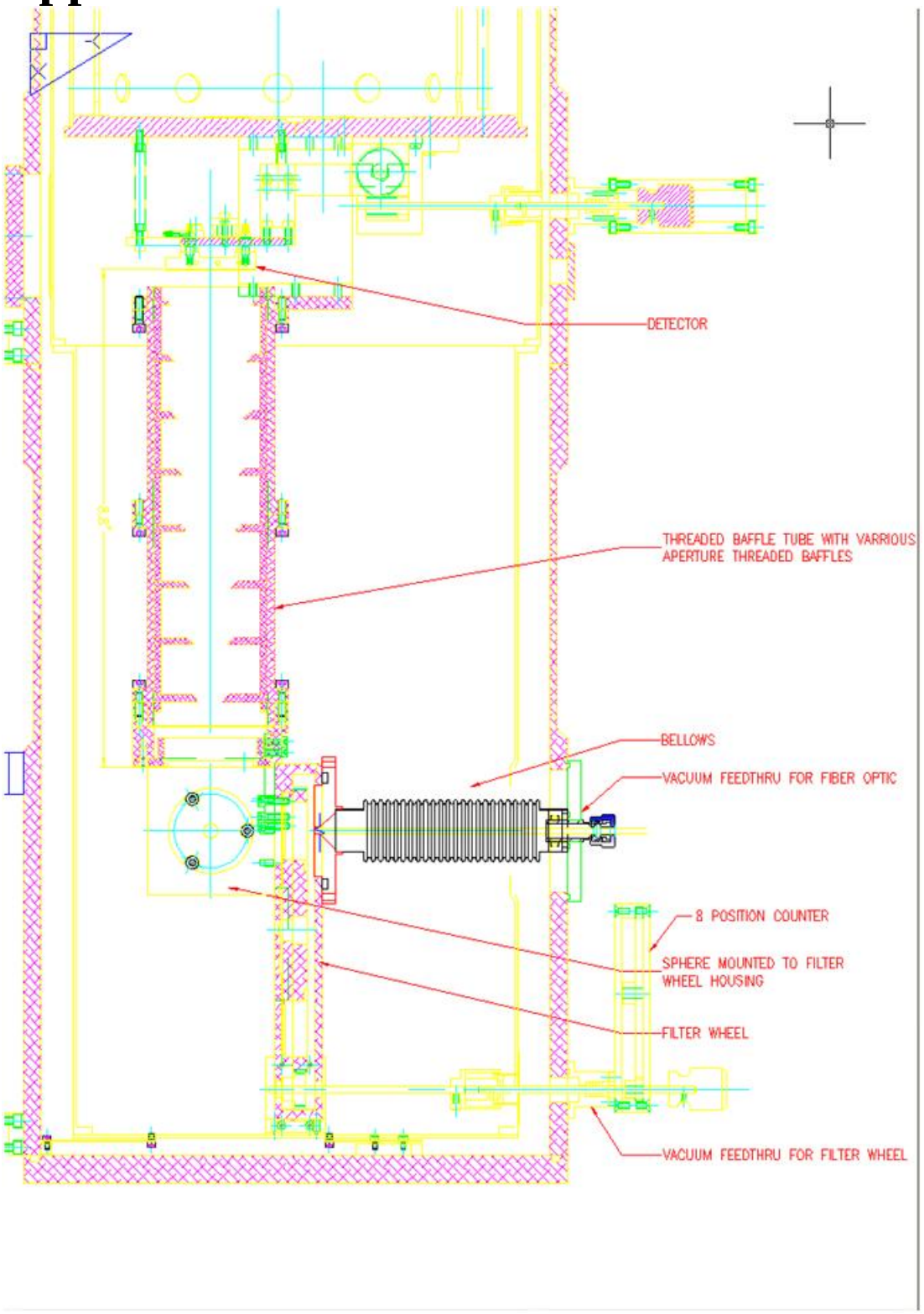
DETECTOR
THREADED BAFFLE TUBE WITH VARRIOUS APERTURE THREADED BAFFLES
BELLOWS
VACUUM FEEDTHRU FOR FIBER OPTIC
8 POSITION COUNTER
SPHERE MOUNTED TO FILTER WHEEL HOUSING
FILTER WHEEL
VACUUM FEEDTHRU FOR FILTER WHEEL

Appendix C

Extension Disassembly

1. Remove glass rod

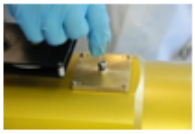


2. Remove DEWAR lid

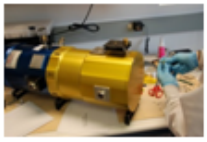


3. Remove bottom thermal support on face plate

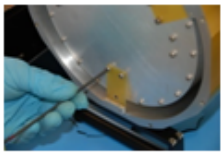
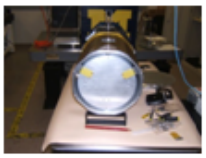

4. Remove screws on perimeter, brace lid to ease strain on system

5. Remove screws for thermal supports (center of faceplate)


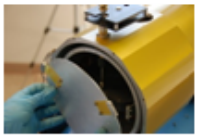

6. Raise mechanical feedthrough shaft

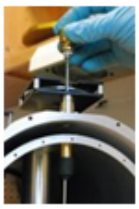

Extension Disassembly

7. Remove photodiode connections (actual steps vary based on the photodiode)



8. Slide the extension case over the cold shield


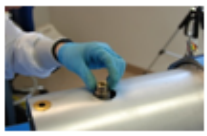

9. Remove the small copper baffle

10. Remove the cold shield


11. Remove the attached assembly, comprised of the: Filter Wheel, Integrating Sphere, and Baffle Tube, from the brackets attached to the cold plate